RF Desensitization in Wireless Devices

Chulsoon Hwang

Additional information is available at the end of the chapter

Abstract

The Internet of Things (IoT), where data are exchanged via wireless connection between devices, is rapidly becoming inextricable from our daily lives. A variety of IoT devices ranging from smart homes to autonomous vehicles and health care have grown explosively. While wireless communication makes the devices conveniently connected, it also makes them inherently vulnerable to electromagnetic interference (EMI). Any radio frequency (RF) antenna used as a radio receiver can easily pick up the unintended electromagnetic noise from integrated circuits (ICs) populated within the same device. The radio range is limited by interference, called RF desensitization, which in turn often limits the usefulness of IoT devices. While the amount of EMI can be estimated using numerical simulations tools like HFSS and CST, engineering issues such as where to place the IC or setting the radiation specification of the IC cannot be so easily addressed. In this chapter, an insightful and efficient RF desensitization model necessary to estimate EMI levels on RF antennas will be addressed. The approach will be focused on two representative areas: noise radiation source modeling and coupling estimation associated with an embedded RF antenna.

Keywords: radio frequency, desensitization, electromagnetic interference, wireless devices, dipole moment, reciprocity

1. Introduction

Electromagnetic interference (EMI) is the disruption of operation of an electronic device when it is in the vicinity of an electromagnetic field in the radio frequency (RF) spectrum caused by another electronic device. Any electronic device generates electromagnetic energy, usually over a wide band of frequencies [1]. These emissions can interfere with the performance of sensitive wireless receivers nearby, called RF desensitization. In

general, as contribution of thermal noise is much lower than that of electromagnetic noise in EMI, only electromagnetic noise is considered. When the noise sources and receivers are situated within the same device or system in which the interference tends to be much more severe than typical EMI. For instance, the noise picked up by AM or FM radio is often a major source of user complaints in the automotive industry. Recently, two popular electric cars, the BMW i3 and Tesla Model X, have excluded terrestrial AM radio because electromagnetic noise from the electric motor interferes with the broadcast reception [2]. The study and analysis of EMI in electronic systems is not a new topic, it has been studied for several decades; but RF desensitization has received renewed interest in recent years as more electronic applications move to wireless communication platforms represented by the Internet of Things (IoT). In recent IoT devices, the noise-sensitive RF antennas are combined with noisy digital integrated circuits (ICs) so the radio range is often limited by the RF desensitization. For instance, the RF module in smart phones composed of an RF antenna, and its receiver can detect signals as weak as −120 dBm in a 200 KHz bandwidth, if not disturbed by nearby electronics. However, the clock frequencies of a smart phone can reach GSM 880–1800 MHz, as well as Bluetooth and Wi-Fi bands [3]. This limits the receiver's ability to detect low-level signals, thus, reducing the overall range and data rate. The radio range limitation of mobile devices often causes great inconvenience to countless consumers. **Figure 1** depicts the typical scenario of a communication system with the receiver's sensitivity affected by electromagnetic noise from in-device components.

A typical industry's product design development cycle starts by defining the product specification and then begins the research and development process. A prototype is populated, debugged, and tested. Based on company protocol, one version of it (prototype, beta, or final product) is tested, and then mitigated and retested—most often many times over—in order to achieve the specification. Any RF desensitization problems that come up late in the design process may be impossible to fix and adding redundant shielding structures entails increased product costs. However, most studies have been focused on understanding the particular EMI problems in a developed system and developing effective numerical simulation methods. In
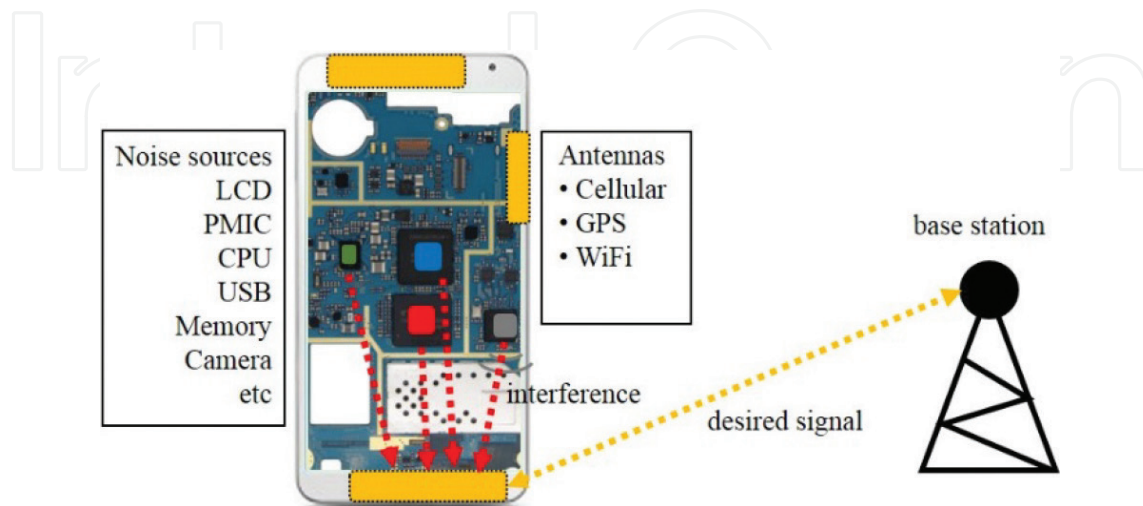
**Figure 1.** Typical RF desensitization mechanism in wireless devices.

addition, the analysis and understanding have been based on their particular physical structures without a universal model to explain the radiation and coupling physics. As IoT devices become increasingly integrated and cost-sensitive, it is essential to have an efficient and fast way to understand the problem not only to mitigate the noise coupling but also to estimate the RF desensitization early in the design cycle, well before a design is fully finished. For this reason, the model should be highly simplified and fast as an early estimation, while also containing physical insight. At the same time, it should not require detailed information such as circuits and physical structures of the noise source, which are the most likely not available in the development stage. This chapter addresses an efficient RF desensitization model to understand the physics of interference within a device, which can also be used as a tool for efficient product design.

2. RF desensitization model

2.1. Noise source model

In contrast to conventional EMI problems where electrically large EMI antenna structures typically exist, ICs have been identified as a major noise source in wireless devices for receiver sensitivity degradation. Today's use of multilayer PCBs allows the designer to move the potential radiation-critical traces on the quasi-shielded inner layers and uses stripline technology to minimize the emission. As a result, especially at higher frequencies, the ICs situated in outer layers start to dominate the electromagnetic emission. The inclusion of ICs as the EMI antenna changes the nature of the problem. Recently, highly developed products, multiple ICs from different suppliers are integrated, and only the circuit/layout related to input/output (IO) are shared outside the IC supplier. As internal circuits are their intellectual properties, it is not allowed to peek into internal circuits of ICs for any reasons. Despite its physical insight, identifying the EMI antenna structure and tracing down the current path are not often feasible for the ICs as it entails knowing proprietary information of the IC itself. Thus, the noise source models to be developed should never use proprietary information or layout of ICs, but yet need to generate the same fields.

Thevenin or Norton source models are fundamental approaches for noise source modeling; the electromagnetic emissions from traces can be modeled by equivalent lumped source/impedance at the end of the traces. With the nature of highly developed electronic products, including all geometry with each dedicated source is not only too computationally intensive, but also entails knowing intellectual property of the IC suppliers. To conceal the detailed structure of noise source, multiple methods have been proposed including multipole expansion, neural networks, and modal expansion. Recently, for the simplicity and rapidity of the modeling and simulation, an equivalent dipole moment method has been investigated [4–6]. Any wire carrying current on it can be represented as an infinitesimal antenna structure known as a Hertzian dipole, or simply called a dipole moment source. ICs are then substituted by a set of magnetic and/or electric dipole moments disposed in the XY-plane which radiates the same electromagnetic field as the original source as shown in **Figure 2**. The
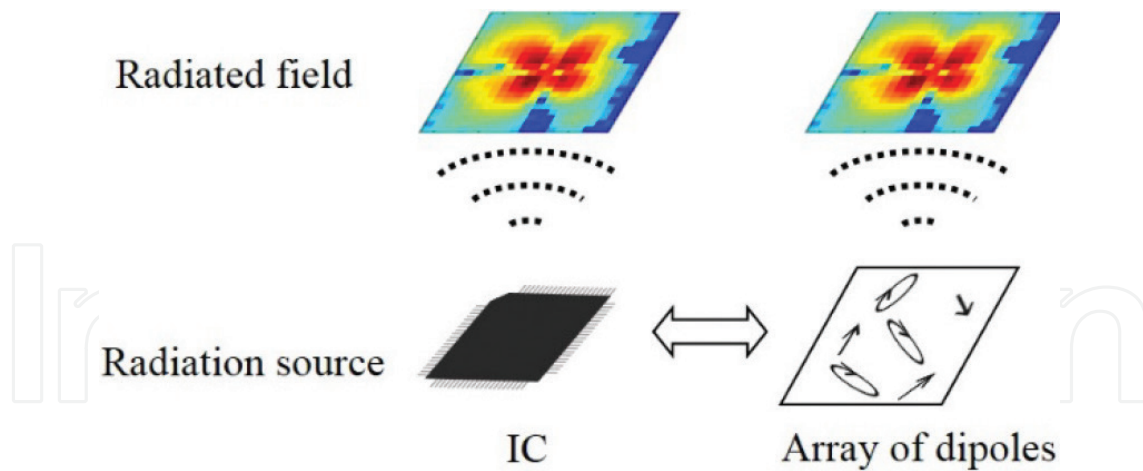
Figure 2. Equivalent radiation model based on a set of Hertzian dipoles.

radiation at a certain observation point of the space is an addition of the emissions of all the sets of dipole moments. The dipole moment source model is versatile as it contains radiation physics, at the same time it does not require knowing any internal circuit geometry. The validity of the dipole moment source model to be used for RF desensitization was experimentally proven by using a practical cell phone [7, 8]. A transfer function between the dipole moment source and RF antenna was experimentally measured and used to represent the EMI coupling to the RF antenna. The transfer function was experimentally measured in [8]. A model to theoretically explain the coupling mechanism and transfer function is addressed in the next subchapter.

The dipole moment source model needs to be reconstructed from measurements as numerical simulations or analytical methods using IC information that is not often available as mentioned before. There are two approaches: using TEM cell with known transfer function and using near-field scanning. Once the fields guided by the TEM cell with dipole moment excitation are known, the dipole moment source can be reconstructed from a dual port TEM cell or GTEM cell measurement. However, as it requires a dedicated board that fits into the opening area of the TEM cells, which is inefficient in terms of costs and time, the near-field scanning method has become the most popular method in industry. In order to reconstruct the dipole moment source from the measured near-field data, the inverse problem needs to be solved. First, electric and magnetic dipoles are assumed as infinitesimal linear wires (straight and circular, respectively) with very small (l « λ), very thin (a « λ), and assuming constant current against the spatial variation. Three types of dipoles (Pz, Mx, and My) are to be considered as the rest of them (Px, Py, and Mz) do not practically radiate by existence of the ground plane and image theory. Then, the fields radiated by the current element can be calculated from the two-step procedure; it is required to determine first A and F, a magnetic vector potential and electric vector potential, respectively, and then find the electric and magnetic fields. The vector potentials from current element and electromagnetic fields from the vector potentials from the Maxwell's equations are given as:

$$\vec{A} = \hat{z}\,\frac{\mu}{4\pi}\,\frac{e^{-j\beta R}}{R}\,P_z\,\Delta l \quad \vec{F} = \hat{x}\,\frac{\varepsilon}{4\pi}\,\frac{e^{-j\beta R}}{R}\,M_x\,\Delta l + \hat{y}\,\frac{\varepsilon}{4\pi}\,\frac{e^{-j\beta R}}{R}\,M_y\,\Delta l, \tag{1}$$

$$H_A = \frac{1}{\mu} \nabla \times A \quad E_A = -j\omega A - j\frac{1}{\omega\mu\varepsilon} \nabla(\nabla \cdot A), \tag{2}$$

$$E_F = -\frac{1}{\varepsilon} \nabla \times F \quad H_F = -j\omega F - \frac{j}{\omega\mu\varepsilon} \nabla(\nabla \cdot F). \tag{3}$$

As the electric and magnetic fields have a linear relationship with each dipole moment, the dipole moment source can then be reconstructed from the radiated electromagnetic field by solving the linear inverse problem. Near-field scanning is often performed on a plane above the noise and source as shown in **Figure 3**.

The relationship between the dipole moment sources and the radiated fields can be represented as shown below.

$$F_n = T_{nk} X_k \tag{4}$$

$$F_n = \begin{pmatrix} [E_x]_{M^2\times 1} \\ [E_y]_{M^2\times 1} \\ [H_x]_{M^2\times 1} \\ [H_y]_{M^2\times 1} \end{pmatrix} = \begin{bmatrix} f_1 \\ f_2 \\ \vdots \\ f_n \end{bmatrix} \quad T_{nk} = \begin{pmatrix} T_{ExPz} & T_{ExMx} & T_{ExMy} \\ T_{EyPz} & T_{EyMx} & T_{EyMy} \\ T_{HxPz} & T_{HxMx} & T_{HxMy} \\ T_{HyPz} & T_{HyMx} & T_{HyMy} \end{pmatrix}$$

$$= \begin{bmatrix} T_{11} & T_{12} & \cdots & T_{1k} \\ T_{21} & & & \vdots \\ \vdots & & \ddots & \\ T_{n1} & \cdots & & T_{nk} \end{bmatrix} \quad X_k = \begin{pmatrix} [P_z]_{N^2\times 1} \\ [M_x]_{N^2\times 1} \\ [M_y]_{N^2\times 1} \end{pmatrix} = \begin{bmatrix} x_1 \\ x_2 \\ \vdots \\ x_k \end{bmatrix} \tag{5}$$

where $[E_x]$, $[E_y]$, $[H_x]$, and $[H_y]$ are the known x and y components of the electric and magnetic fields obtained from near-field measurement; $[P_z]$, $[M_x]$ and $[M_y]$ are the unknown electric and magnetic dipoles in the dipole array; and, $[T]$ is a known field generation matrix whose expression can be found from Eqs. (1)–(3). The least square method can then be used to reconstruct the dipole moment source as shown below.

$$E(X) = \|T_{nk} X_k - F_n\|^2 = \sum_{i=1}^{n} \left(\sum_{j=1}^{k} T_{nj} X_j - F_i \right)^2 \tag{6}$$

$$\hat{X}_k = [T_{nk}^* T_{nk}]^{-1} T_{nk}^* F_n \tag{7}$$

where T_{nk}^*, conjugate transpose of T_{nk}.

However, because of the nature of inverse problem inherent from mathematical procedure, the solution is very sensitive to noise and is not unique because of the ill-posed transformation matrix relating equivalent sources and the measured near-field data while the noise in the near field scanning measurement is inevitable. In addition, the solution is mathematically drawn so it is not able to capture the radiation physics. Although a non-physical solution can match the
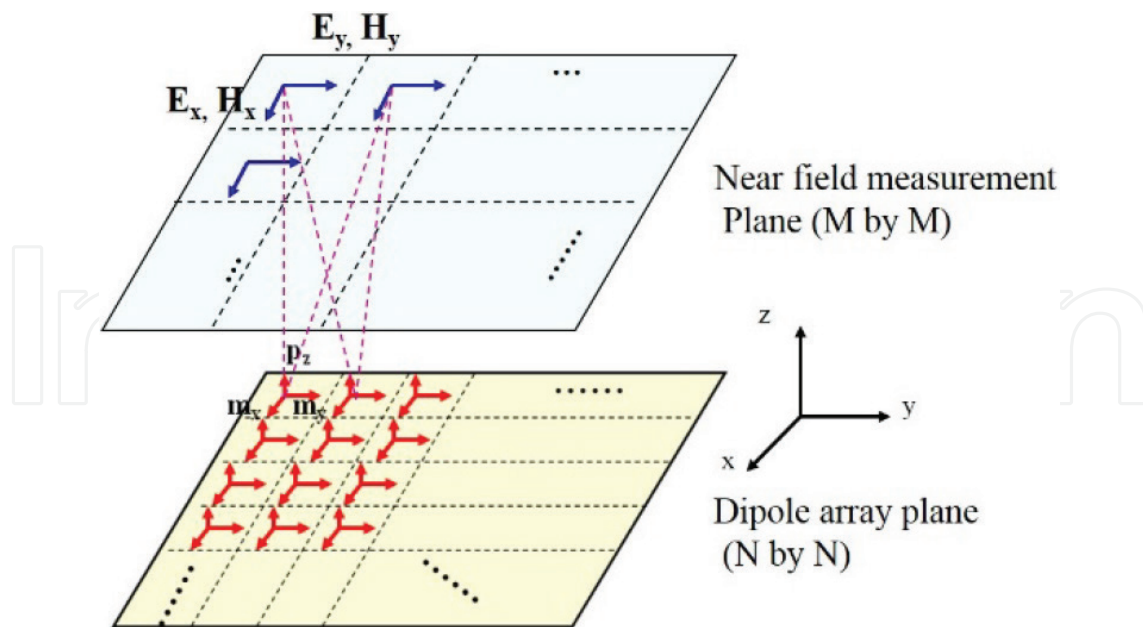
Figure 3. Source reconstruction using near field scanning.

field well at the scanning plane, it often fails to predict the fields well at other locations. In order to overcome the limitation, either a regularization method to minimize the energy of the source or various optimization methods have been investigated. The regularization method has essentially the same inherent problem, and the performance of the optimization algorithms heavily depends on the initial values users provide. Therefore, a more reliable method is needed to reconstruct equivalent dipole moments accurately with physical meaning. In [8], the least square method was used, but the dipole type and location was predetermined based on understanding of the near-field radiation pattern. Then, the least square method was used only to determine the magnitude and phase, rather than all information such as dipole moment types and orientation and, more importantly, the number of dipole moments and their location.

An example of the dipole moment source reconstruction in a practical cellphone based on the understanding of radiation physics, and the near-field radiation pattern is described in details. The structure carrying the high-speed MIPI DSI clock signals is a conductor-backed coplanar waveguide with differential signaling. It has a two layer stack-up; the top layer is ground plane and the bottom layer has four traces: ground, clock+, clock-, ground. **Figure 4** shows the top and bottom side on the edge of the FPCB. The clock lane on the FPCB is routed all the way to the input pins of the DDI chip. There are no significant geometry changes on the bottom side of the FPCB; however, the top of the FPCB has a clear discontinuity. The top of the FPCB has a solid metal and acts as the ground plane, but there is no ground at the edge of the FPCB. The surface current increases at the edge of the top ground plane, which does not come from a conduction path since there is no metal in direct contact with the edge of the top ground plane. Therefore, the only way to generate the increase of the conduction current is from a displacement current path. A simplified illustration of common mode current flow is shown in **Figure 5**. The top view of the current flow shows that there are two current loops facing opposite directions. These two equivalent Mz dipole moments with an equal magnitude, but opposite direction will cancel each other out. The diagram on the right side shows
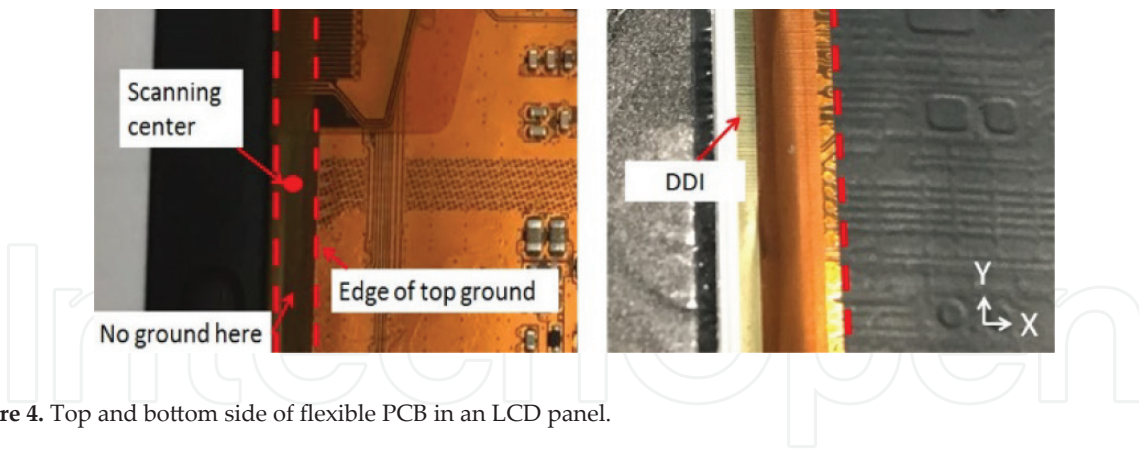
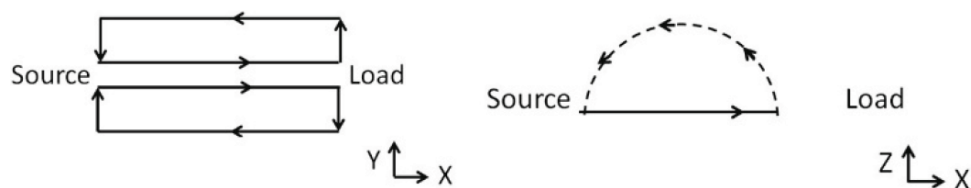**Figure 4.** Top and bottom side of flexible PCB in an LCD panel.

**Figure 5.** Illustration of common mode current flow in a differential clock pair.

the side view of the common mode current flow. The conduction current and the displacement current form a current loop in the *xz* plane. A current loop facing the *y* axis forms an *My* dipole moment, so the radiation source can be modeled as an *My* dipole moment.

In order to reconstruct the radiation source, the near-field above the LCD and FPCB was measured at 897.0 MHz. To obtain the phase resolved H-field data in the near-field, the tuned receiver mode of the VNA was used. In tuned receiver mode, both of the two ports of the VNA are receivers. Two H-field probes were connected to the two receiver ports of the VNA and the H-field probes were calibrated to get the probe factor which included the magnitude and phase information of the probe and the connecting cables and amplifiers. The cell phone controlled the LCD panel in the ON state during the whole near-field measurement to ensure the clock lane was active. The scanning height was 1 mm above the FPCB. The reference probe was placed near the noise source so that the reference signal had enough signal-to-noise ratio (SNR).

The measured H-field pattern at 897.0 MHz is shown in **Figure 6**. For all of the field patterns, the center of field pattern plot lies in the physical center of the scanning plane. This indicates that the noise source came from the clock lane because the scanning center was located exactly above it. A magnetic dipole moment along the *y* axis is denoted as M_y. The magnitude and phase of the equivalent dipole moment M_y can be easily obtained using the least square method as given in Eqs. (6) and (7). The H-field patterns from reconstructed dipole moment source are shown and the magnitude and phase from the reconstructed M_y dipole moment agree well with the magnitude and phase of the measured H-field patterns from the cell phone.

By containing physics prior to the source reconstruction, the reconstructed dipole moments were able to represent the radiation physics. However, the location and types of dipole
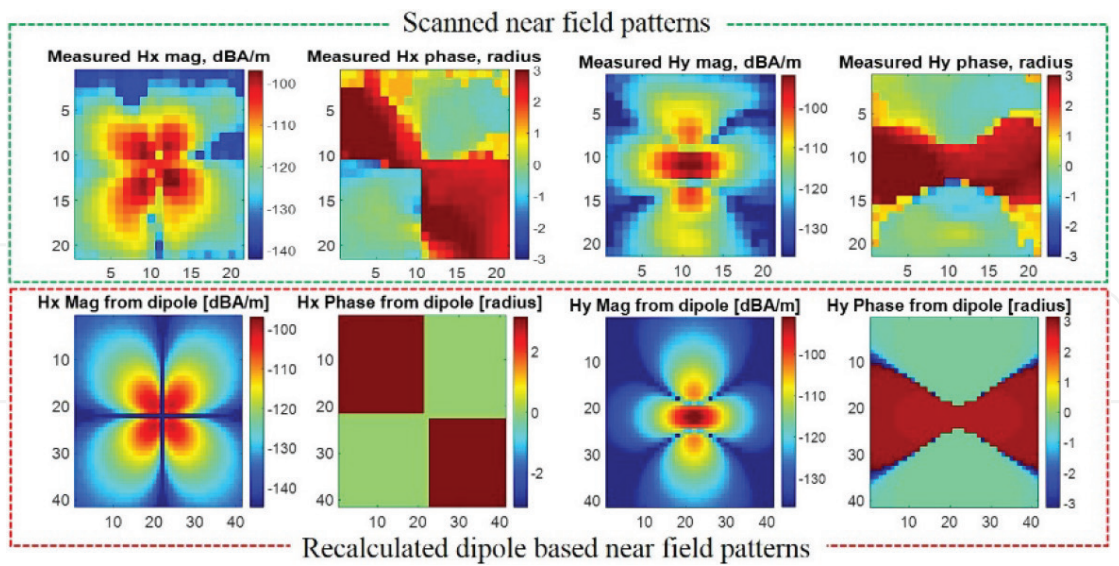
Figure 6. Comparison between scanned near-field patterns and calculated near-field patterns from reconstructed dipole moment source.

moment were determined from the researcher's educated guess based on understanding of dipole moment radiation, which is not suitable to disseminate the developed methodology to industry. The near-field pattern of each dipole moment is shown in **Figure 7**. It requires understanding of dipole moment radiation to recognize the location and type of dipole moment from the radiation patterns; sometimes it is not even possible, especially when multiple dipole moments exist. For this case, the physical dipole can be reconstructed based on the radiation pattern recognition, and the recognition can be automated by artificial intelligence based on machine learning algorithm [9].

2.2. Coupling model

As the radiation from an IC is independent of the environment nearby (this is usually the case except for the special cases such as IC noise modulation studied in [10]), the noise coupling
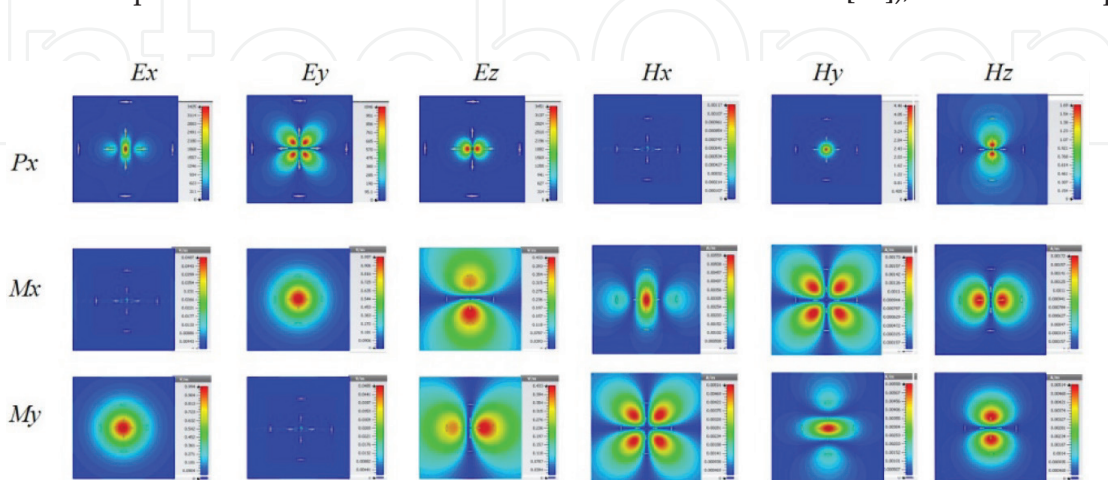
Figure 7. Near field pattern of each dipole moment.

canvbe decomposed into two parts: radiation and coupling. While conventional studies have focused on the analysis of radiation physics for debugging, recently, understanding of the coupling mechanism and its modeling have received more attention for EMI-aware design. For the coupling modeling, the Friis transmission equation could be used, but it only works for the far-field region. Since coupling problems occurring in electronic devices are strongly relevant to near-field, estimating the coupling by the Friis equation may cause the wrong results. Instead, the coupling decomposition method based on reciprocity with Huygens' box is a fundamental approach to decompose the noise coupling. It models the noise source and coupling independently, then combines them using the Lorentz reciprocity theorem, which allows separate investigations on each part. However, using Huygens' box blurs the physical meaning of the noise source so it fails to provide physical insight for the design. In this section, an efficient coupling model using dipole moment source and reciprocity will be introduced; this method can contain radiation physics and, thereby, provide an efficient tool for analysis and design for RF desensitization.

The reciprocity theorem states that when places of voltage and current sources in any reciprocal network are interchanged, the amount or magnitude of current and voltage flowing in the circuit remains the same, as depicted in **Figure 8**. In other words, Z_{21} is identical to Z_{12} in reciprocal networks.

This theorem also applies to electromagnetics. When two sources $(\vec{J}_1, \vec{M}_1)$ and $(\vec{J}_2, \vec{M}_2)$ exist in the same region, electromagnetic fields by reaction theory $(\vec{E}_1, \vec{H}_1)$ and $(\vec{E}_2, \vec{H}_2)$ must satisfy the Lorentz reciprocity theorem, whose simplified integral form is:

$$\iiint_V \left(\vec{E}_1 \cdot \vec{J}_2 - \vec{H}_1 \cdot \vec{M}_2 \right) dv = \iiint_V \left(\vec{E}_2 \cdot \vec{J}_1 - \vec{H}_2 \cdot \vec{M}_1 \right) dv. \tag{8}$$

When three current density or electromagnetic fields are known, the rest can be calculated from the abovementioned equation, which leads to the core idea for this approach. For instance, if one source, $(\vec{J}_1, \vec{M}_1)$ and both electromagnetic fields on two locations, $(\vec{E}_1, \vec{H}_1)$ and $(\vec{E}_2, \vec{H}_2)$, are known, the rest, $(\vec{J}_2, \vec{M}_2)$, can be calculated analytically.

Using Eq. (8), the original noise coupling problem from **Figure 9** can be decomposed into two parts, the forward problem and the reverse problem (from **Figure 10**). The currents $\vec{J}_s^{fwd}$, $\vec{M}_s^{fwd}$ describe the noise source in the forward problem, where the victim antenna is terminated. In the reverse problem, the noise source is removed and the victim antenna radiates. $\vec{J}_a^{rev}$, $\vec{M}_a^{rev}$ are currents on the victim antenna and the corresponding fields on the location of the original noise source are denoted as $\vec{E}_s^{rev}$, $\vec{H}_s^{rev}$. Then, Eq. (8) can be rewritten as:

$$\iiint_V \left(\vec{J}_s^{fwd} \cdot \vec{E}_s^{rev} - \vec{M}_s^{fwd} \cdot \vec{H}_s^{rev} \right) dv = \iiint_V \left(\vec{J}_a^{rev} \cdot \vec{E}_a^{fwd} - \vec{M}_a^{rev} \cdot \vec{H}_a^{fwd} \right) dv. \tag{9}$$

The subscript "s" and "a" represent the source and antenna, respectively (**Figures 9–11**).

As the electric and magnetic dipole moments (denoted as P and M) are essentially identical to the volume integral of electric and magnetic current density (J and M), respectively, derivation from the Lorentz reciprocity theorem can be simplified to a simple and straightforward form. The
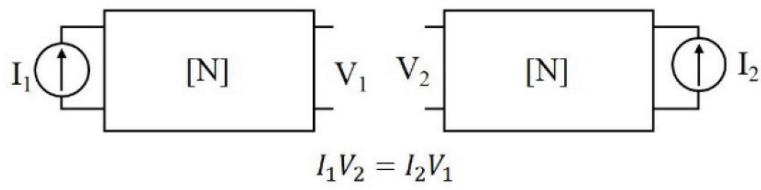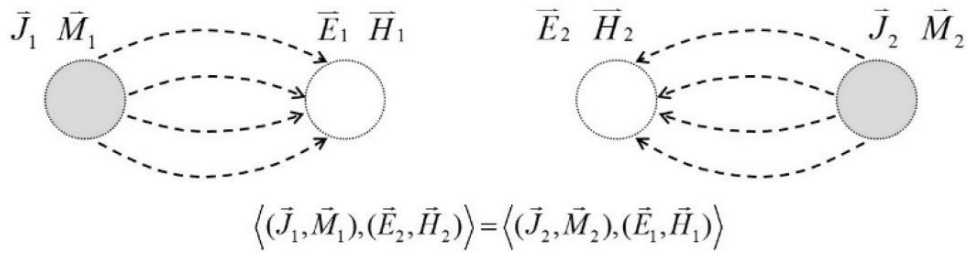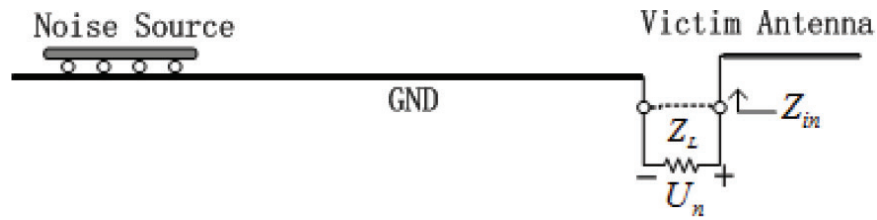
Figure 8. Reciprocity theorem.

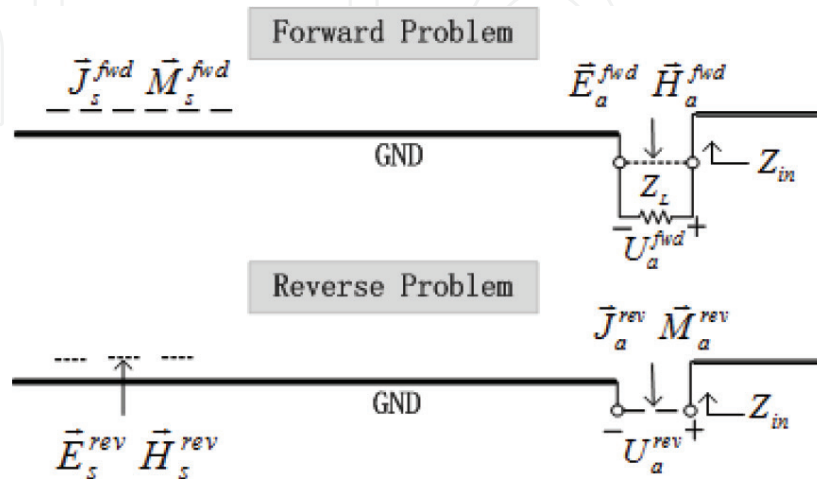**Figure 9.** Original RF desensitization problem.

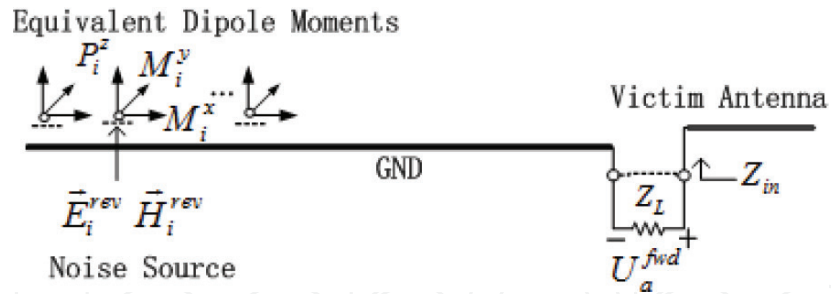**Figure 10.** Decomposed problem; forward and reverse problem.

Figure 11. Equivalent RF desensitization model using dipole moments and reciprocity.
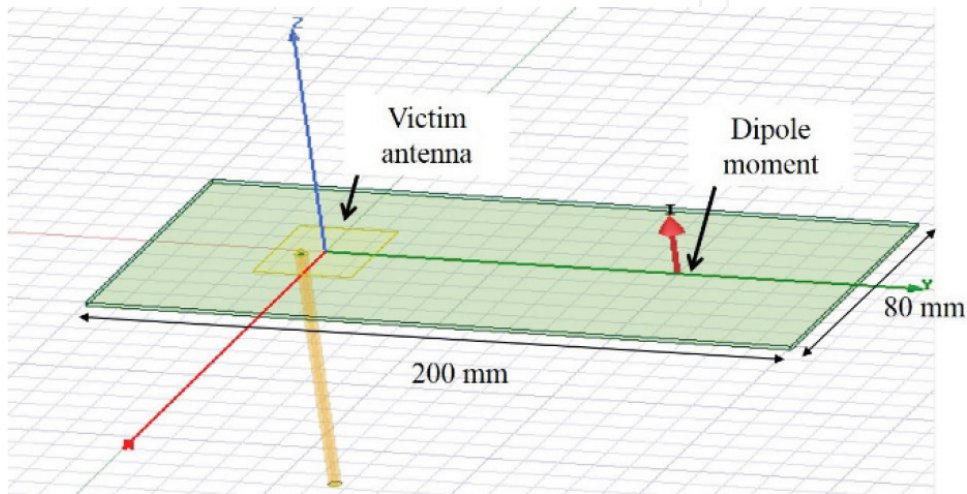

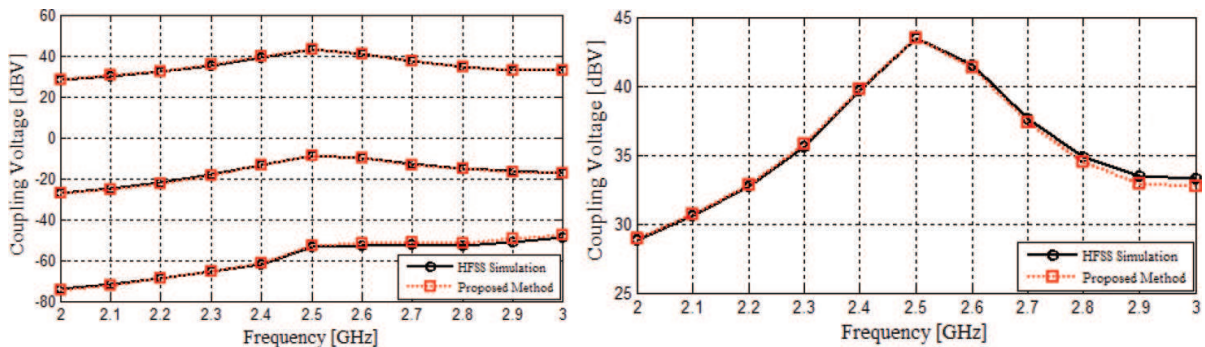**Figure 12.** Model for the numerical validation; a single P_z excitation is shown as an example.

Figure 13. Numerical validation with a single dipole moment (left) and a combination of three kinds of dipoles (right).

left side of the Lorentz reciprocity theorem states the relationship between the fields generated by the victim antenna and the current density represent the IC. As the fields can be assumed as constant across the current density area, the left side of the equation can be simplified as:

$$\iiint_V \left(\vec{E}_s^{rev} \cdot \vec{J}_a^{fwd} - \vec{H}_a^{rev} \cdot \vec{M}_a^{fwd} \right) dv = \iiint_{V_s} \left(\vec{E}_s^{rev} \cdot \vec{J}_a^{fwd} - \vec{H}_a^{rev} \cdot \vec{M}_a^{fwd} \right) dv$$

$$= \sum_{i=1}^{N} \iiint_{V_i} \left(\vec{E}_a^{rev} \cdot \vec{J}_a^{fwd} - \vec{H}_a^{rev} \cdot \vec{M}_a^{fwd} \right) dv = \sum_{i=1}^{N} \left(\vec{E}_i^{rev} \cdot \vec{P}_i^{fwd} - \vec{H}_i^{rev} \cdot \vec{M}_i^{fwd} \right), \tag{10}$$

where N represents the number of dipoles used to model the noise source. Note that the letter M used in the reciprocity theorem represents magnetic current density defined in Maxwell's equation, while the letter M used in the final equation represents the magnetic dipole moment. The unit of the magnetic dipole moment is $V \cdot m$ because the magnetic dipole is derived by integrating the magnetic current density, which is different from $A \cdot m^2$ derived from an electric current loop in [11]. Basically, an arbitrary electrically small source can be replaced by six kinds of dipoles based on the multiple expansion of a radiation source. When the radiation source is located close to a large ground plane, which is the usually the case in modern electronic devices, the radiation from tangential electric dipoles and vertical magnetic dipoles is canceled by their images. Therefore, in Cartesian coordinates, the vertical electric dipoles P_z and tangential magnetic dipoles M_x and M_y are enough to represent the noise source.

The right side of the Lorentz reciprocity theorem (Eq. (9)) is associated with electromagnetic fields and current density on the cross section of the antenna port, which is typically a good transmission line. As voltage and current are well defined in a transmission line (i.e., TEM mode), the field and current density can be changed to voltage and current quantities as [12]:

$$\iiint_V \left(\vec{J}_a^{\,rev} \cdot \vec{E}_a^{\,fwd} - \vec{M}_a^{\,rev} \cdot \vec{H}_a^{\,fwd} \right) dv = -\left(\frac{1}{Z_{in}} + \frac{1}{Z_L} \right) U_a^{fwd} U_a^{rev}, \tag{11}$$

where Z_L is the load impedance of the victim antenna in the forward problem, which is usually 50 ohm. Z_{in} is the input impedance of the victim antenna in the reverse problem. u_a^{fwd} is the voltage coupled on the victim antenna in the forward problem. u_a^{rev} is the voltage excited on the victim antenna in the reverse problem.

Substituting Eqs. (10) and (11) into Eq. (9) gives [13]

$$U_a^{fwd} = \frac{Z_{in} Z_L}{U_a^{rev}(Z_{in} + Z_L)} \sum_{i=1}^{N} \left(-P_i^z \left(\hat{z} \cdot \vec{E}_i^{\,rev} \right) + M_i^x \left(\hat{x} \cdot \vec{H}_i^{\,rev} \right) + M_i^y \left(\hat{y} \cdot \vec{H}_i^{\,rev} \right) \right). \tag{12}$$

From an engineering perspective, a transfer function concept can be defined based on Eq. (12) to quantify the coupling relationship from each dipole moment to the victim antenna as

$$U_a^{fwd} = \sum_{i=1}^{N} \vec{f}_{P_i} \cdot \vec{P}_i + \sum_{i=1}^{N} \vec{f}_{M_i} \cdot \vec{M}_i \tag{13}$$

$$\vec{f}_{P_i} = -\frac{Z_{in} Z_L}{U_a^{rev}(Z_{in} + Z_L)} \vec{E}_i^{\,rev} \quad \vec{f}_{M_i} = \frac{Z_{in} Z_L}{U_a^{rev}(Z_{in} + Z_L)} \vec{H}_i^{\,rev}, \tag{14}$$

where $\vec{f}_{P_i}$ is a transfer function representing the coupled noise from each electric dipole moment $\vec{P}_i$. $\vec{f}_{M_i}$ is a transfer function representing the coupled noise from each magnetic dipole moment $\vec{M}_i$. There are two important observations: the transfer function has a linear relationship with its respective E- and H-field, and the transfer functions can be obtained as long as the respective E- and H-field are acquired in the reverse problem. Thus, the coupling voltage on the victim antenna can be expressed by the linear superposition of the product of equivalent

dipole moments and the corresponding electromagnetic fields. The final form is simple, but describes the coupling mechanism quite intuitively. It states that the coupling is simply proportional to the fields (when the victim antenna radiates) on the IC location and different fields contribute depending on the type of IC radiation. This understanding can greatly improve the design procedure. Detailed radiation structures do not necessarily need to be known to understand the RF desensitization problems; even with a brief information of noise source (type and orientation), the characteristics of RF desensitization can be fully understood and the EMI level can be quantitatively estimated, which will provide an efficient design tool and facilitate pre-layout design.

Several simple models were created in the full-wave simulation tool, HFSS, to validate the proposed method. In these models, a single dipole moment was treated as the noise source. The victim antenna is a 28 mm × 37 mm patch antenna that has a center frequency designed to 2.5 GHz. In these models, $P_z = 1A \cdot m$, $M_x = 1V \cdot m$ and $M_x = 1V \cdot m$ are used, respectively. Based on the proposed method, only the field in the reverse problem needs to be scanned and then the coupling voltage can be calculated by using Eqs. (13) and (14). For comparison, the coupling voltage was also obtained directly from simulation.

In the comparison, the typical error of the proposed method was less than 0.1 dB. The maximum error reached 1.4 dB for dipole M_y at 2.8 GHz. The differences were introduced by numerical errors in the reverse problem. Three field values needed for the calculations, E_z, H_x, and H_y, were obtained by running one simulation (the reverse problem). However, the H_y component at the noise source location was significantly smaller than the other fields (E_z and H_x), which meant H_y was more prone to numerical errors than the other cases, and consequently resulted in the largest error. On the other hand, that is the reason why the M_y case had the lowest coupling voltage. For a source containing three kinds of dipole moments at the same time, the model also showed a good correlation with the maximum error of 0.6 dB at 3 GHz.

2.3. Practical applications

The RF desensitization model was applied to estimate the noise coupling from an LCD panel to an RF antenna in a practical cell phone. The cell phone under test consisted of three parts: a LCD, a main body, and a FPCB which connected the two together. There are two antennas on the cell phone: main antenna and sub antenna as illustrated in **Figure 14**. The high-speed MIPI DSI signals routed on the FPCB can be potential noise sources and couple to the cellular antenna. At the edge of the FPCB, a discontinuity of the ground plane was observed as explained in the previous section. The conduction current and the displacement current formed a current loop in the *xz*-plane. A current loop facing the *y*-axis formed an M_y dipole moment, thus, the radiation source was modeled as an M_y dipole moment.

A three-step process was performed to validate the RF desensitization model in this cell phone measurement [14]. The coupled noise from the LCD panel to the antennas was estimated using the model and later compared with direct measurement results.

In step one, the LCD was put into working condition. The radiation source was on and near-field scanning was conducted. Through the process described in the previous section, the
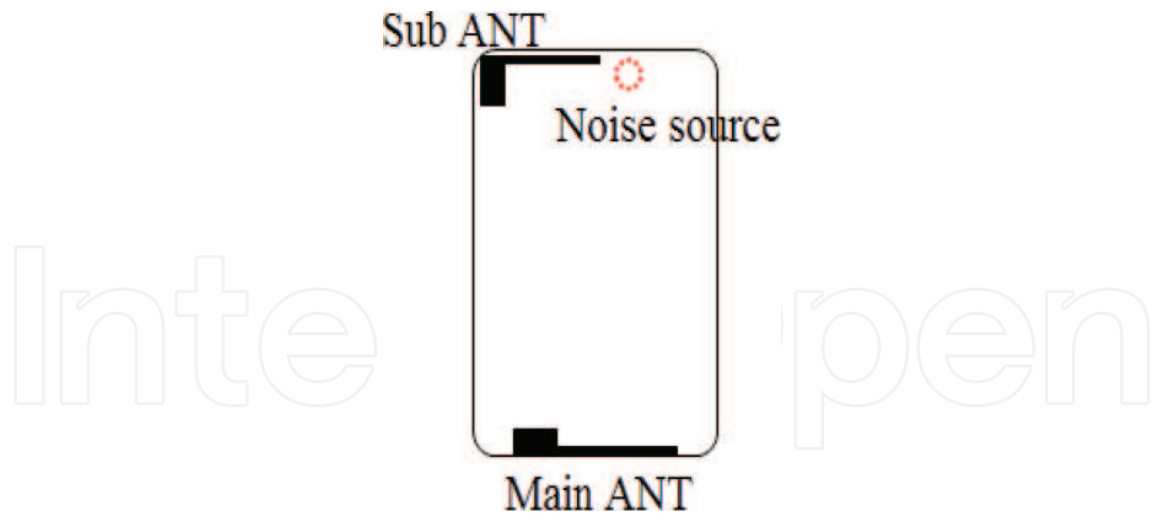
Figure 14. DUT illustration.

dipole moment was reconstructed. The comparison between the measured near-field pattern and the calculated near-field pattern from the reconstructed source is shown in **Figure 6** .

In step two, the antenna radiated in the reverse problem. Because only magnetic dipole My existed in this problem, only the y-component of the H-field was needed to estimate coupled voltage according to the inner product in Eqs. (13) and (14). In this problem, Eqs. (6) and (7) can be further simplified to:

$$U_a^{fwd} = \vec{f}_M \cdot \vec{M} \ = \ \frac{Z_{in} Z_L}{U_a^{rev}(Z_{in} + Z_L)} H_y^{rev} M_{y'} \tag{15}$$

where H_y^{rev} was measured using a near-field H-probe. The H-field was converted from S-parameter measurement through a probe calibration. In the reverse problem, port one was connected to the victim antenna for excitation, port two was connected to the H-field probe. An S_{21} measurement was needed to measure the transfer function from a unit magnetic dipole M_y to the victim antenna. The set-up for the reverse problem is shown in **Figure 15**. Theoretically, H_y^{rev} should be measured at the exact location of the equivalent dipole moment M_y which is often inside an IC. In reality, the H-field probe often cannot be put inside an IC because of physical constraints. Here, the H-field probe was placed as close to the location of the dipole moment as possible. In order to test robustness of measurement set-up, the H-field probe was moved up several mm to test the variation of the measured H-field; the results were within 1 dB.

After finishing steps 1 and 2, M_y in the forward problem and H_y in the reverse problem were obtained. Using Eq. (15), the coupled voltage on the antenna port was analytically calcu-lated. In step 3, direct measurement of the coupled power was performed to compare with the estimated coupled value. As the noise source is from the clock harmonics of 448.5 MHz, the whole process was repeated for the first seven harmonics of the fundamental frequen-cies. The proposed method was used to calculate the coupled power at the main antenna port
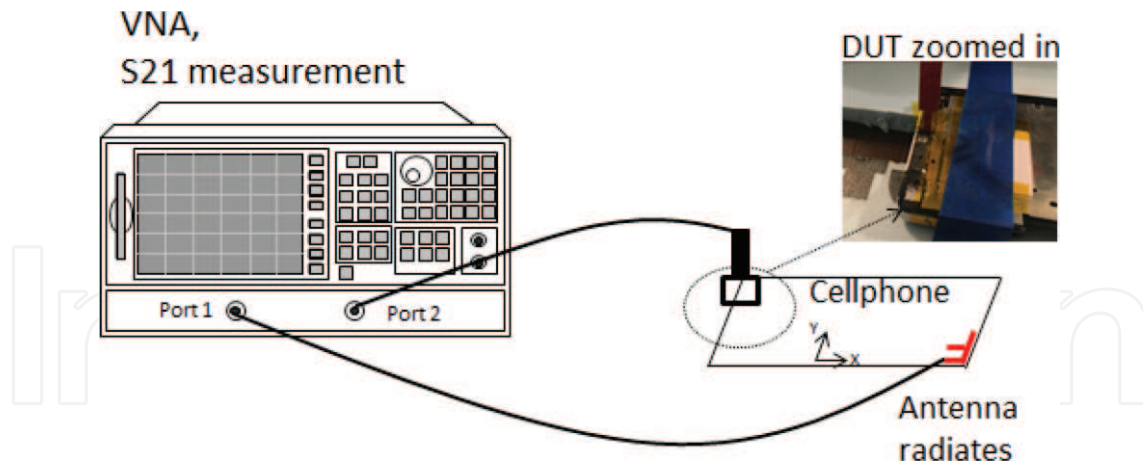
Figure 15. Measurement set-up for the reverse problem.

for the first seven harmonics. Estimated results were compared with measurement results, as shown in **Figure 16**. Besides the main antenna, there was another sub antenna in this cell phone. The same procedures were performed to estimate the coupled power through the forward and reverse problems. The estimated coupled power from the proposed method was compared with measurements. For both of the antennas, estimation errors were mostly within 5 dB, which is acceptable for most engineering practices. The proposed method was successfully validated through the measurements using a practical cell phone.

In engineering practice, engineers often need to know how much improvement a certain change will give. This method can help engineers answer that question and make accurate and fast decisions. As mentioned, RF desensitization problems contain two parts: the noise source and the coupling to an antenna. Recently, a lot of work has been done to build equivalent source modeling to understand the noise source. However, the coupling to the antenna is widely believed to be difficult and unpredictable. A transfer function concept was introduced to quantify the coupling from each unit dipole moment to the antenna. In the beginning, the transfer functions are analytically derived from reciprocity theorem, but it turns out that the transfer functions are relatively easy to obtain in both simulations and measurements.
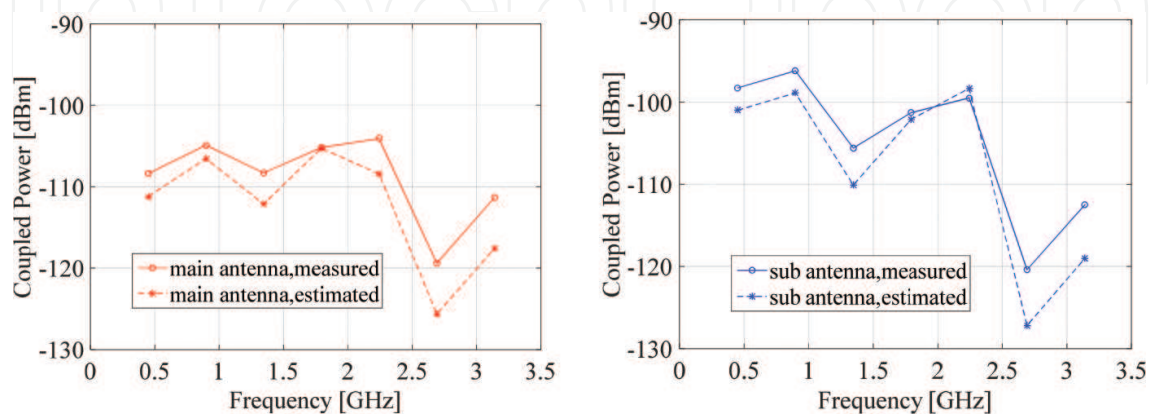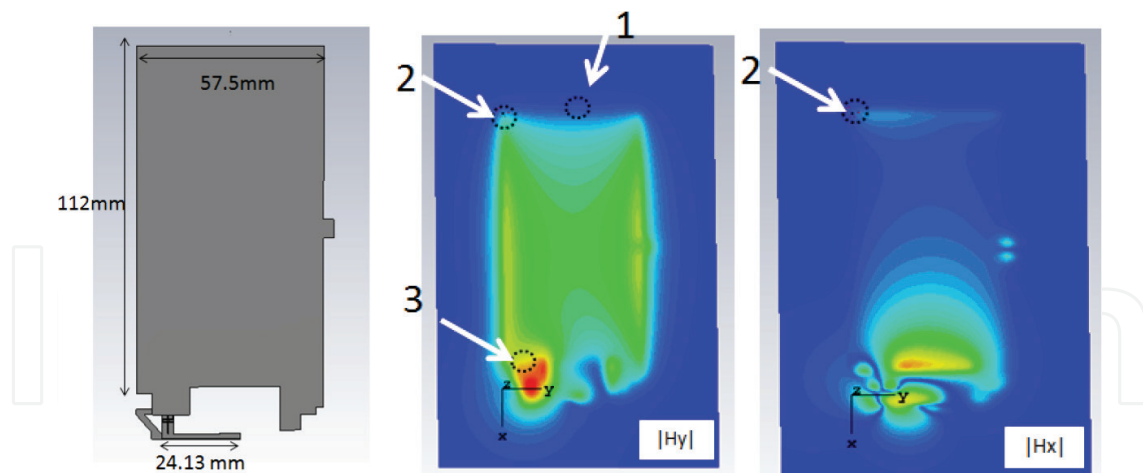

Figure 16. Measured and estimated coupled power to the antennas.

Figure 17. A typical cell phone antenna model (left), magnitude of H_y when the antenna radiates (center), and magnitude of H_x when the antenna radiates (right).

One example is to find the best placement of the IC to minimize RF desensitization. For example, a cell phone and its antenna model are shown in **Figure 17**. The simulated magnitude of H_y and H_x at 1 GHz are shown when the antenna radiates. If the noise source was identified as a M_y dipole moment, according to Eqs. (13) and (14), the transfer function from each unit M_y dipole moment to the victim antenna was proportional to H_y in the reverse problem. So out of the given locations 1, 2 and 3, location 1 had the smallest transfer function and location 3 had the largest transfer function. From the RF desensitization perspective, location 1 will be the best place to locate the noise source M_y dipole moment where the coupling between the M_y dipole moment to the victim antenna is the smallest.

The RF desensitization model can also help understand the effect of the noise source rotation. For example, suppose the noise source is fixed at location 2. By rotating the noise source 90°, the M_y dipole moment becomes an M_x dipole moment. According to Eqs. (13) and (14), the transfer function from each unit M_x dipole moment to the victim antenna is proportional to H_x in the reverse problem. Since H_x is much weaker than H_y, the transfer function is much weaker after rotating the noise source by 90°. So for this particular antenna at 1 GHz, rotating the original noise source by 90° will help reduce RF desensitization a lot.

3. Conclusions

In this chapter, an efficient model to understand and mitigate the RF desensitization problem was discussed. As IoT devices are required to increase their radio range, it is essential to understand the mechanism of RF desensitization. A fundamental understanding of EMI noise coupling and having an efficient tool to address this problems early in the design cycle can achieve a fast and low-cost product design. A dipole moment-based reciprocity method was introduced to estimate the RF desensitization problem. Its formulas were analytically derived from Maxwell equations and the reciprocity theorem. Using the derived equations, we clearly identified which part of the equation belonged to the noise source itself and which part belonged to the coupling

path of the antenna. A transfer function concept was also introduced to quantify the coupling coefficient from each unit dipole moment to the victim antenna. The transfer functions can be relatively easy to obtain from either simulation or measurement. Using this RF model, we can provide RFI/EMI engineers with a clear idea about what goes wrong and how to fix it.

Author details

Chulsoon Hwang

Address all correspondence to: hwangc@mst.edu

Missouri University of Science and Technology, Rolla, MO, USA

References

[1] Ott HW. Electromagnetic Compatibility Engineering. Hoboken: Wiley; 2009. 872 p. DOI: 10.1002/9780470508510

[2] Motherboard. Why Electric Cars Are Ditchng AM Radio [Internet]. 2016. Available from: https://motherboard.vice.com/en_us/article/yp3vmj/why-electric-cars-are-ditching-am-radio [Accessed: January 10, 2018]

[3] Scogna A, Shim H, Yu J, Oh C-Y, Cheon S, Oh N, Kim DS. RFI and receiver sensitivity analysis in mobile electronic devices. In: Proceedings of Designcon; Santa Clara, CA. January 28–February 2, 2017

[4] Vives-Gilabert Y, Arcambal C, Louis A, de Daran F, Eudeline P, Mazari B. Modeling magnetic radiations of electronic circuits using near-field scanning method. IEEE Transactions on Electromagnetic Compatibility. 2007;**49**(2):391-400. DOI: 10.1109/TEMC.2006.890168

[5] Tong X. Simplified equivalent modelling of electromagnetic emissions from printed circuit boards [thesis]. University of Nottingham; 2010

[6] Yu Z, Koo J, Mix JA, Slattery K, Fan J. Extracting physical IC models using near-field scanning. In: Proceedings of IEEE International Symposium. On Electromagnetic Compatibility; July 26-30, 2010; Fort Lauderdale, FL. 2010. pp. 317320

[7] Cho GY, Jin J, Park HB, Park HH, Hwang C. Assessment of integrated circuits emissions with an equivalent dipole moment method. IEEE Transactions on Electromagnetic Compatibility. 2017;**59**(2):633-638. DOI: 10.1109/TEMC.2016.2633332

[8] Huang Q, Zhang F, Enomoto T, Maeshima J, Araki K, Hwang C. Physics based dipole moment source reconstruction for RFI on a practical cellphone. IEEE Transactions on Electromagnetic Compatibility. 2017;**59**(6):1693-1700. DOI: 10.1109/TEMC.2017.2705641

[9] Huang Q, Chen Y, Hwang C, Fan J. Machine learning based source reconstruction for RF desensitization analysis. In: Proceedings of Designcon 2018; Santa Clara; January 28–February 2, 2018

[10] Hwang C, Pommerenke D, Fan J, Enomoto T, Maeshima J, Araki K. Modeling and estimation of LCD noise modulation for radio frequency interference. IEEE Transactions on Electromagnetic Compatibility. 2017;**59**(6):1685-1692. DOI: 10.1109/TEMC.2017.2705178

[11] Wilson P. On correlating TEM cell and OATS emission measurements. IEEE Transactions on Electromagnetic Compatibility. 1995;**37**(1):1-16. DOI: 10.1109/15.350235

[12] Richmond JH. A reaction theorem and its applications to antenna impedance calculations. IRE Transactions on Antennas and Propagation. 1961;**9**(6):515-520. DOI: 10.1109/TAP.1961.1145068

[13] Lee S, Zhong Y, Huang Q, Enomoto T, Seto S, Araki K, Fan J, Hwang C. Analytical intra-system EMI model using dipole moments and reciprocity. In: Proceedings of IEEE International Symposium On Electromagnetic Compatibility; May 14-17, 2018; Singapore. 2018

[14] Huang Q, Enomoto T, Maeshima J, Araki K, Fan J, Hwang C. Accurate and fast RFI prediction based on dipole moment sources and reciprocity. In: Proceedings of Designcon; 2018; Santa Clara. January 28–February 2, 2018